How to cite: *Angew. Chem. Int. Ed.* **2024**, *63*, e202312135
doi.org/10.1002/anie.202312135

Cluster Catalysis | Hot Paper

Dual Catalysis of Gold Nanoclusters: Photocatalytic Cross-Dehydrogenative Coupling by Cooperation of Superatomic Core and Molecularly Modified Staples**

Katsuhiro Isozaki, Kenta Iseri, Ryohei Saito, Kyosuke Ueda, and Masaharu Nakamura**

Dedicated to Professor Shigeru Yamago on the occasion of his 60th birthday

Abstract: Thiolate-protected gold nanoclusters (AuNCs) have attracted significant attention as nano-catalysts, revealing a superatomic core and gold-thiolate staples as distinct structural units. Here, we demonstrate the unprecedented dual catalytic activity of thiolate-protected $[Au_{25}(SR)_{18}]^-$ nanoclusters, involving both photosensitized $^1O_2$ generation by the Au_{13} superatomic core and catalytic carbon-carbon bond formation facilitated by $Au_2(SR)_3$ staples. This synergistic combination of two different catalytic units enables efficient cross-dehydrogenative coupling of terminal alkynes and tertiary aliphatic amines to afford propargylamines in high yields of up to 93%. Mixed-ligand AuNCs bearing both thiolate and alkynyl ligands revealed the intermediacy of the alkynyl-exchanged AuNCs toward both photosensitization and C–C bond-forming catalytic cycles. Density functional theory calculations also supported the intermediacy of the alkynyl-exchanged AuNCs. Thus, the use of ligand-protected metal nanoclusters has enabled the development of an exceptional multifunctional catalyst, wherein distinct nanocluster components facilitate cooperative photo- and chemo-catalysis.

Introduction

Ligand-protected gold nanoclusters (AuNCs) have received enormous attention as nanocatalysts because of their distinct electronic structure and remarkable size-dependent properties, setting them apart from conventional gold nanoparticles.[1,2] In particular, thiolate-protected AuNCs have been extensively studied to gain insights into the structure–property relationship by synthesizing various AuNCs with well-defined molecular formulas.[1c,2a,e] Single-crystal X-ray structural analyses revealed that thiolate-protected AuNCs consist of a superatomic core with closed-shell electron configurations and multiple gold-thiolate staples surrounding the core.[2a,b,e] Although the superatomic core and staples couple with each other via multiple metallic Au–Au bonds, they can behave as two or more individual molecular units. This was elucidated by femtosecond relaxation dynamics studies of photoexcited $[Au_{25}(SR)_{18}]^-$ clusters, revealing different decay pathways from the Au_{13} superatomic core and six $Au_2(SR)_3$ staples surrounding the core forming the parent Au_{25} cluster.[3,4] In addition, recent studies of phosphine- or N-heterocyclic carbene (NHC)-protected Au_{13} nanoclusters revealed that Au_{13} superatomic cores within $[Au_{25}(SR)_{18}]^-$ possess a similar photophysical properties with the ligand-protected Au_{13} nanoclusters, despite the different surface environments of their Au_{13} superatomic cores.[5] Therefore, both phosphine-/NHC-protected Au_{13} nanoclusters and $[Au_{25}(SR)_{18}]^-$ form triplet excited states and emit a similar near-infrared phosphorescence derived from the HOMO–LUMO excitation of their Au_{13} superatomic cores, suggesting their potential application as photosensitizers to generate singlet oxygen as well as photocatalysts for the autooxidation of sulfides and amines (Figure 1a).[1a,b,5a,b,6–8] Recently, we reported a supramolecular reaction field effect of peptide dendron thiolates on the surface of $[Au_{25}(SR)_{18}]^-$, which can accelerate the photocatalytic oxidation of amino alcohols, primarily via intermolecular hydrogen bonds between the peptide moiety of the thiolate ligands and substrates.[8] In this photocatalytic reaction, the Au_{13} superatomic core played a crucial role in the singlet oxygen ($^1O_2$) photosensitization. In contrast, surface Au atoms in the staples did not participate in the catalytic transformation, merely anchoring the peptide dendron thiolate ligands to form a supramolecular reaction field. These results also anticipate

[*] Dr. K. Isozaki, K. Iseri, R. Saito, K. Ueda, Prof. Dr. M. Nakamura
International Research Center for Elements Science, Institute for Chemical Research, Kyoto University
Uji, Kyoto 611-0011 (Japan)
and
Department of Energy and Hydrocarbon Chemistry, Graduate School of Engineering, Kyoto University
Nishikyo-ku, Kyoto 615-8510 (Japan)
E-mail: kisozaki@scl.kyoto-u.ac.jp
masaharu@scl.kyoto-u.ac.jp

[**] A previous version of this manuscript has been deposited on a preprint server (https://doi.org/https://doi.org/10.21203/rs.3.rs-3191053/v1).

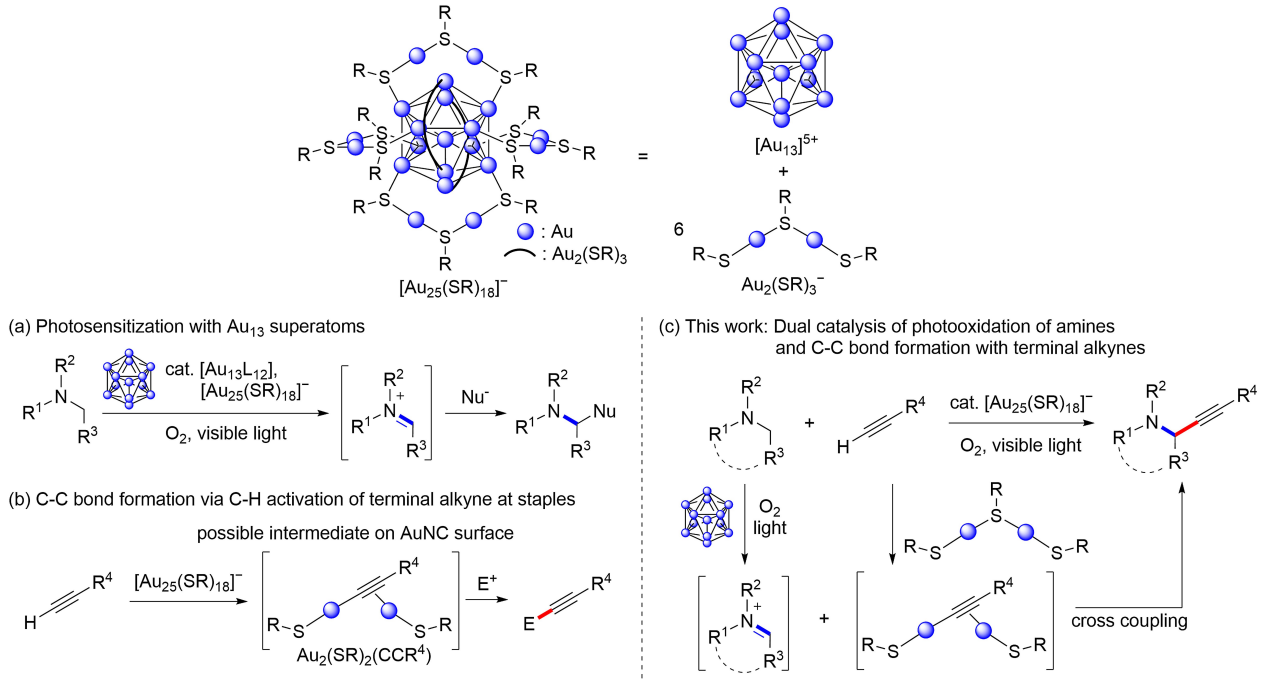

Figure 1. (a) Photosensitization with Au_{13} superatoms. (b) C–C bond formation via C–H activation of terminal alkyne at staples. (c) Dual catalysis of photooxidation of amines and C–C bond formation with terminal alkynes with $[Au_{25}(SR)_{18}]^-$.

that the Au_{13} superatomic cores serve as stable scaffolds, retaining their original photophysical properties even when surrounded by different surface-protecting molecules, such as gold-thiolate staples within $[Au_{25}(SR)_{18}]^-$.

Furthermore, thiolate-protected AuNCs have participated in various catalytic reactions,[1] including various chemical transformations of alkynes, such as hydroamination,[9] Huisgen cycloaddition,[10] A^3 coupling,[11] and C–H carboxylation.[12] These catalytic reactions demonstrate similar reaction mechanisms, with the surface Au atoms within the staples acting as the catalytic center upon structural changes in the AuNCs, such as ligand detachment from the staple moiety. Recently, Ackerson et al. reported that the reaction of $[Au_{25}(SR)_{18}]^-$ with alkynyl metal compounds leads to the formation of nanoclusters with partially exchanged ligands, denoted as $[Au_{25}(SR)_{18\text{-}x}(alkynyl)_x]^-$.[13] The structural similarity between thiolate- and alkynyl-protected metal nanoclusters (MNCs) implies that alkynyl ligands replace thiolate ligands in the staples during the ligand-exchange reaction.[2c,d] This suggests the possible intermediacy of alkynyl-exchanged MNCs as catalytically active species in the catalytic reactions of alkynes, which can be formed via thiolate exchange with terminal alkyne substrates within the staples (Figure 1b). In contrast to the ligand exchange occurring in the staples during catalytic reactions, the superatomic core is protected by the staples, thus only electronically affecting the catalytic activity without structural perturbation. This observation is supported by the doping effect on the catalytic activity of $[MAg_{24}(SR)_{18}]^-$ nanoclusters toward C–H carboxylation.[12] The distinct functionalities of the superatomic core and staples led us to envision their divergent roles as separate structural components in photocatalytic reactions.

Herein, we report the pioneering dual catalytic activity of gold nanoclusters, enabling cross-dehydrogenative coupling between tertiary amines and terminal alkynes via photooxidation catalysis leveraging the photosensitization properties of the Au_{13} superatomic core and C–C bond-forming catalysis driven by the reactivity of gold-thiolate staples (Figure 1c). The first-generation peptide dendron thiolate-functionalized AuNCs, referred to as **DOP1-AuNC** or $[Au_{25}(S\text{-}DOP1)_{18}]^-$, where DOPx represents dendritic ornithine peptide and x denotes the dendron generation, showed higher catalytic activity than that of the conventional phenylethanthiolate-protected AuNCs, referred to as **PET-AuNC** (Figure 2). The intermediacy of alkynyl-exchanged AuNCs was confirmed through reaction studies, demonstrating that newly synthesized alkynyl-exchanged AuNCs showed comparable photosensitization properties and catalytic activity to **DOP1-AuNC** in cross-dehydrogenative coupling, even at a short induction period. Density functional theory (DFT) study of the reaction pathway using the model AuNC $[Au_{25}(SMe)_{17}(C{\equiv}CPh)]^-$ revealed the thiolate ligand within a staple undergoing exchange with the alkynyl ligand derived from the substrate, providing further evidence supporting the potential intermediacy of alkynyl-exchanged AuNCs. Our work demonstrates the promising potential of ligand-protected MNCs as multifunctional catalysts, showing both photocatalytic properties based on the superatomic core and simultaneous catalytic capabilities of the staple moieties.

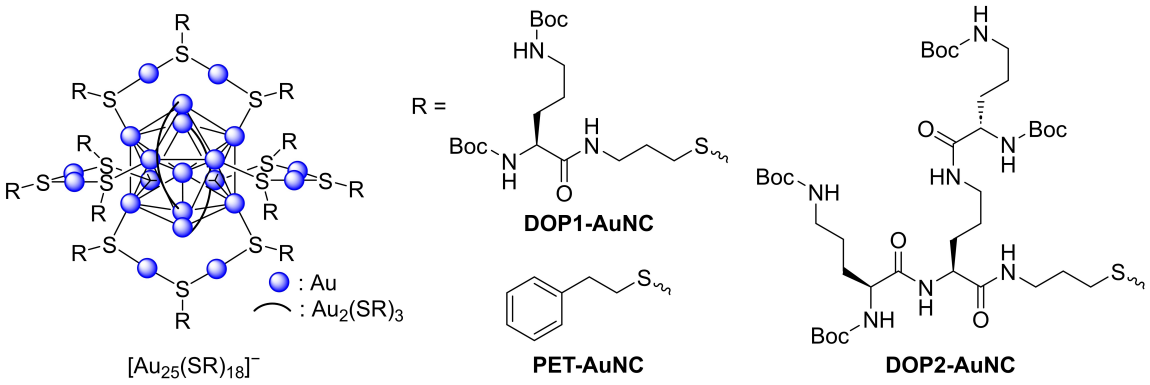

Figure 2. Molecular structure of AuNC catalysts.

Results and Discussion

Screening of different reaction conditions

The study began with a meticulous screening of the reaction conditions (Table 1). Through cross-coupling of *N*-butylpyrrolidine (**1a**) and 4-ethynylanisole (**2a**), regioselective synthesis of propargylamine **3aa** was achieved, yielding a racemic product with 29 % yield. This reaction was facilitated by the use of a catalytic amount of **DOP1-AuNC** when irradiated with visible light at 680 nm under an oxygen atmosphere for 60 h (Table 1, entry 1). The reaction did not proceed in the absence of oxygen, light, or the AuNC catalyst (Table 1, entries 2–4). The irradiation at 680 nm induced electron excitation within the Au_{13} superatomic core of **DOP1-AuNC**, generating singlet oxygen, as reported in our previous work.[8] Thus, these results reveal the dual catalytic activity of **DOP1-AuNC**, facilitating both the photocatalytic oxidation of amine **1a** and the subsequent catalytic C–C bond formation between the iminium intermediate and alkyne **2a**. When non-hydrogen-bonded **PET-AuNC** was used as the catalyst, the product yield decreased to 16 % (Table 1, entry 5). However, the addition of the acetyl-protected **DOP1-SAc** did not further improve the yield of **PET-AuNC** (Table 1, entry 6). These contrasting results clarify the positive effect of the supramolecular reaction field associated with the first-generation peptide dendron on the photocatalytic reaction, similar to our previous report.[8] Upon the addition of the second-generation peptide dendron thiolate-functionalized Au_{25} nanocluster, referred to as **DOP2-AuNC**, the expected product **3a** was not obtained despite the complete consumption of the amine **1a** (Table 1, entry 7). This result suggests that the strong hydrogen bonding nature of the second-generation peptide dendron[8] enables the reaction product to be strongly entrapped within the reaction field. Thus, the catalyst is rendered ineffective or "poisoned". The low product yield in this reaction was attributed to the slow exchange of the alkyne substrate and hydrogen-bonded product within the reaction field. This issue was addressed by employing 10 times higher concentrated conditions, resulting in a substantially increased product yield of 91 %. However, a longer reaction time of 344 h was required (Table 1, entry 8).

Table 1: Screening of different reaction conditions.

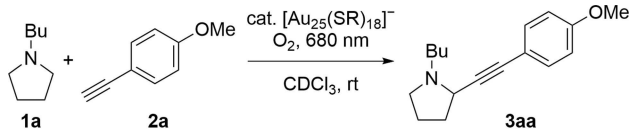

entry	catalyst	yield (%)
1	**DOP1-AuNC**	29
2[b]	**DOP1-AuNC**	trace
3[c]	**DOP1-AuNC**	n.d.
4	no cat.	n.d.
5	**PET-AuNC**	16
6	**PET-AuNC + DOP1-SAc**	16
7	**DOP2-AuNC**	n.d.
8[d]	**DOP1-AuNC**	91

[a]Reaction conditions: **1a** (12 μmol), **2a** (6.0 μmol), **DOP1-AuNC** (1 mol %), O_2 (1.0 atm), light (680 nm, 3.3–3.7 mW/cm^2), $CDCl_3$ (0.6 mL). Yield was determined by ^{1}H NMR using an internal standard when **1a** was completely consumed. [b]Under Ar. [c]In dark. [d]100 μM.

Substrate scope of amines and alkynes

The substrate scope of different amines was investigated under the optimized reaction conditions. *N*-Alkyl pyrrolidines **1a**, **1b** and tetrahydroisoquinoline **1c** were efficiently converted into the corresponding propargylamines **3aa**, **3ba**, and **3ca** with exceptional regioselectivity and high yields of 91, 92, and 93 %, respectively (Table 2). The alkynylation of *N*-aryl tetrahydroisoquinoline **1d** also provided the corresponding alkynylated product **3da** with a yield comparable to previous cases. Furthermore, *N*-alkyl piperidine **1e** and morpholine **1f** exclusively formed *N*-propargyl piperidine **3ea** and morpholine **3fa**, exhibiting yields of 66 and 61 %, respectively. In addition, trialkylamines, such as triethylamine (**1g**), benzyldimethylamine (**1h**), and *N*, *N*-dimethyl-L-phenylalanine methyl ester (**1i**), also participated in the reaction, providing the corresponding *N*-propargyl products **3ga**, **3ha**, and **3ia**, respectively. For pyrrolidines and

Table 2: Scope of amine substrates.

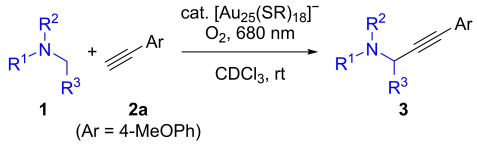

entry	substrate	product	yield (%)
1	**1a**, R = Bu	**3aa**	91 (29)
2	**1b**, R = Me	**3ba**	92 (42)
3	**1c**, R = Me	**3ca**	93 (44)
4	**1d**, R = Ph	**3da**	(44)
5	**1e**, Y=CH_2	**3ea**	66 (20)
6	**1f**, Y=O	**3fa**	61 (21)
7	**1g**	**3ga**	91 (39)
8	**1h**	**3ha**	(40)
9	**1i**	**3ia**	48
10	**L-1j**	**L-3ja**	57
11	**D-1j**	**D-3ja**	57

[a]Reaction conditions: **1a** (0.12 mmol), **2a** (60 μmol), **DOP1-AuNC** (1 mol %), O_2 (1.0 atm), light (680 nm, 3.3–3.7 mW/cm^2), $CDCl_3$ (0.6 mL). Yield was determined by ^{1}H NMR using an internal standard when **1** was completely consumed. Parentheses: ^{1}H NMR yield with 10 mM condition.

tetrahydroisoquinolines, the cross-coupling reaction occurs at the α-position of the cyclic amine because of the easily oxidizable nature of these ring skeltons.[14] In contrast, for piperidine and trialkylamines, cross-coupling exclusively takes place at the sterically less hindered *N*-methyl groups rather than at the benzyl and α-position of the amino acids which form thermodynamically more stable iminium intermediates, similar to a previous report on the oxidative cyanation of tertiary amines using singlet oxygen.[15] This regioselectivity strongly depends on steric hindrance, underscoring the involvement of single-electron transfer followed by hydrogen atom transfer (SET/HAT), leading to the formation of iminium intermediates at the sterically less hindered positions.[16] Additionally, aniline derivatives, such as *N*,*N*-dimethylaniline and *N*-phenylpyrrolidine, and amide, 1-butylpyrrolidin-2-one remained unoxidized under given reaction conditions because of their low nucleophilicity to form exciplexes with singlet oxygen.[17] Similarly, quinuclidine was not oxidized. Although primary and secondary amines, such as 1-octylamine and dibutylamine were oxidized by singlet oxygen to afford the corresponding imines, they did not yield the target products as the reactivity of the imines was lower than that of the iminium intermediates. The effect of the supramolecular reaction field was investigated using L-/D-GlyPhe dipeptides **L-/D-1j**, as they were expected to form intermolecular hydrogen bonds with peptide dendron ligands. However, no discernible kinetic resolution was observed between the L- and D-GlyPhe dipeptides, resulting in identical time-course profiles and product yields (Figure S2). These findings suggest that intermolecular interactions between peptide dendrons and amino acids do not affect the enantio-differentiation.

Furthermore, the scope of alkyne substrates was also investigated (Table 3). When employing diluted reaction conditions, arylalkynes carrying electron-donating substituents, such as *p*-, *o*-methoxy, and *p*-methyl groups, actively participated in the reaction to afford the coupling products **3aa**, **3ac**, and **3ad** in 29, 19, and 14 % yields, respectively. In contrast, no coupling product was obtained when using *m*-methoxyphenylacetylene (**2b**), suggesting the higher reactivity of electron-rich alkynes due to the resonance effect

Table 3: Scope of alkyne substrates.

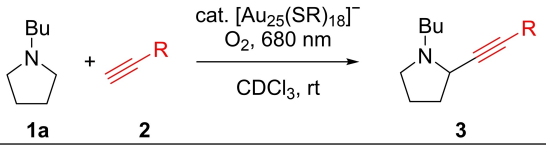

entry	substrate	product	yield (%)
1	**2a**, R' = *p*-OMe	**3aa**	91 (29)
2	**2b**, R' = *m*-OMe	**3ab**	(n.d.)
3	**2c**, R' = *o*-OMe	**3ac**	(19)
4	**2d**, R' = *p*-Me	**3ad**	(14)
5	**2e**, R' = H	**3ae**	85 (n.d.)
6	**2f**, R' = *p*-CO_2Me	**3af**	86 (8)
7	**2g**, R' = *p*-F	**3ag**	92 (13)
8	**2h**, R' = *p*-Cl	**3ah**	62 (trace)
9	**2i**	**3ai**	7 (n.d.)
10	**2j**	**3aj**	71 (n.d.)
11	**2k**	**3ak**	59 (n.d.)
12	**2l**	**3al**	72 (n.d.)

[a]Reaction conditions: **1a** (0.12 mmol), **2a** (60 μmol), **DOP1-AuNC** (1 mol %), O_2 (1.0 atm), light (680 nm, 3.3–3.7 mW/cm^2), $CDCl_3$ (0.6 mL). Yield was determined by ^{1}H NMR using an internal standard when **1a** was completely consumed. Parentheses: ^{1}H NMR yield with 10 mM condition.

induced by electron-donating substituents. Similarly, no coupling products were obtained for phenylacetylene or *p*-chlorophenylacetylene. Notably, alkynes bearing *p*-methoxycarbonyl and *p*-fluoro groups, despite their electron-deficient nature, yielded coupling products **3af** and **3ag** with yields of 8 and 13 %, respectively. This result strongly suggests that the hydrogen-bonding properties of alkynes are crucial for accelerating catalytic reactions. Under optimized 10 times concentrated condition, the product yields of electron-rich **3aa**, electron-neutral **3ae**, electron-deficient **3af**, **3ag** and **3ah** were significantly improved to 91, 85, 86, 92, and 62 %, respectively. However, 2-pyridylacetylene (**2i**) exhibited reduced catalytic activity due to the coordination of pyridine moiety, resulting in a mere 7 % yield of **3ai**. In contrast, 2-thiophenylacetylene (**2j**) produced the corresponding product **3aj** with a yield of 71 %, indicating the absence of any detrimental effects from the thiophenyl ring. Non-arylated alkynes, such as 1-octyne (**2k**) and trimethylsilylacetylene (**2l**), also actively participated in this reaction, producing the corresponding products **3ak** and **3al** in 59 and 72 % yield, thereby expanding the synthetic utility of the current catalytic transformations. In contrast, internal alkynes, such as 4-octyne and tolan (1,2-diphenylacetylene), were fully recovered, suggesting that the deprotonation of terminal alkynes is the key step in this reaction.

Hydrogen bonding properties of the ligands

The formation of intermolecular hydrogen bonds between the peptide dendrons and the amine/alkyne substrates was investigated by ^{1}H NMR spectroscopy (Figure S3–6). In these experiments, amine **1a** and alkyne **2a** were used as guests, while acetyl-protected 1st-generation peptide dendron thiol **DOP1-SAc** and **DOP1-AuNC** were used as host molecules. Both ^{1}H NMR spectra of **1a** and **2a** showed a downfield shift of the methylene protons neighboring the nitrogen atom and the alkynyl terminal proton[18] with increasing concentrations of **DOP1-SAc**, indicating the formation of intermolecular hydrogen bonds (Figure S3 and S5). Notably, when 5.0 mM of **1a** was mixed with 1.0 mM of **DOP1-AuNC**, remarkable downfield shifts of 0.034 and 0.029 ppm were observed for methylene protons (Figure S4). This shift was larger than that using 200 mM of **DOP1-SAc** (Figure S3), revealing the significant impact of peptide dendrons as a hydrogen bonding supramolecular reaction field on AuNC toward amine substrates. In contrast, when 5.0 mM of **2a** was mixed with 1.0 mM of **DOP1-AuNC**, a slight downfield shift of the alkynyl terminal proton at 0.0021 ppm was observed, which is comparable to that using 25 mM **DOP1-SAc** (Figure S5 and S6). Considering that **DOP1-AuNC** has 18 peptide dendron ligands, the comparable binding affinity to **DOP1-SAc** at 25 times higher concentration suggests a negligible enhancement effect of peptide dendrons on AuNCs for intermolecular hydrogen bonding with alkyne substrates. These results uncover the nature of the supramolecular reaction field constructed of peptide dendrons, which primarily act as a hydrogen-bonding donor field, efficiently accommodating amine substrates near the surface of the AuNC catalysts.

Mechanistic studies

Several mechanistic investigations were performed to gain insights into the reaction mechanism. The formation of radical intermediates was confirmed by radical trapping experiments using 2,2,6,6-tetramethylpiperidine 1-oxyl (TEMPO) and 1,4-hydroquinone as radical scavengers (Figure 3a). The addition of TEMPO or 1,4-hydroquinone to the reaction mixture resulted in almost complete inhibition of the photocatalytic reaction, affording only trace amounts of the product, thus, confirming the existence of radical intermediates. This result corresponds well with the observed regioselectivity (Table 2), supporting the SET/HAT mechanism of amine oxidation using photogenerated singlet oxygen. Furthermore, insights into the reactive intermediates in the catalytic cycle were obtained from the time-course reaction profiles monitored using ^{1}H NMR spectroscopy (Figure 3c and d). The reaction profile involving **DOP1-AuNC** revealed the existence of an induction period of 12 h following the initiation of photoirradiation. It is worth noting that our previous study revealed the absence of an induction period for the photocatalytic oxidation of amines.[8] This suggests that the formation of reactive intermediates in the C–C bond formation is crucial for initiating the catalytic cycle. Recently, Ackerson et al.

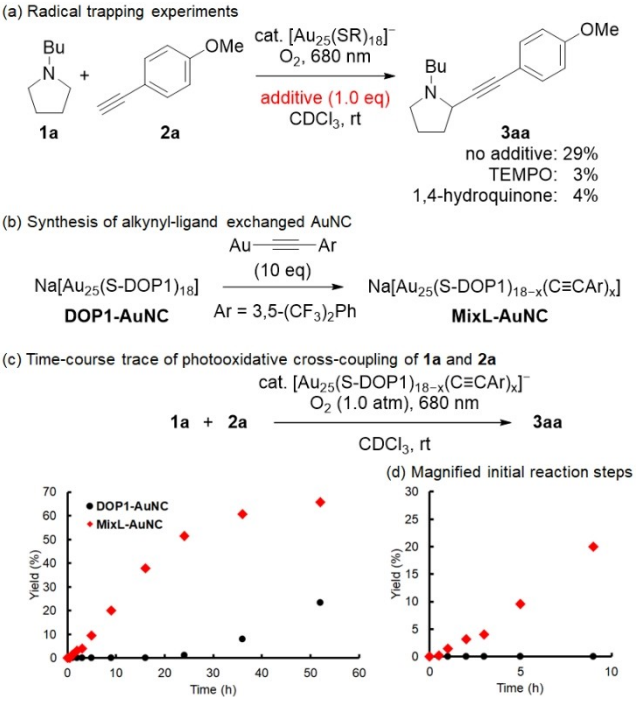

Figure 3. Mechanistic studies. (a) Radical trapping experiments. (b) Synthesis of alkynyl-ligand-exchanged AuNC. (c) Time-course reaction profiles with **DOP1-AuNC** and **MixL-AuNC**. (d) Magnification of the initial reaction steps.

reported that the thiolate ligands of Au_{25} clusters can be replaced by alkynyl ligands.[13] Such alkynyl-exchanged AuNCs are considered to be the reactive intermediates in our photocatalytic reaction and facilitate C–C bond formation with the iminium intermediates. In light of this, AuNCs bearing thiolate ligands and partially exchanged with alkynyl ligands were synthesized using Ackerson's method (Figure 3b).[13] The ligand-exchange reaction was performed by mixing the alkynyl-gold compound with **DOP1-AuNC**, followed by purification using silica gel column chromatography. The partially alkynyl-exchanged AuNCs were obtained as the mixture of deca- to pentadeca-alkynyl-exchanged AuNCs $[Au_{25}(S\text{-}DOP1)_{18\text{-}x}(C{\equiv}CAr)_x]^-$ (averaged substitution number $x = 12.2 \pm 1.5$), referred to as **MixL-AuNC**, whose molecular formula was confirmed using electrospray ionization mass spectroscopy (ESI-MS) (Figure S7). The UV/Vis absorption spectrum showed the existence of a characteristic absorption band originating from the Au_{13} superatomic core at 680 nm, similar to that of the $[Au_{25}(SR)_{18}]^-$ clusters (Figure S8). When **MixL-AuNC** was used as the catalyst, the induction period was significantly shortened to 1 h, suggesting that the alkynyl-exchanged AuNCs actively participated in the catalytic cycle as reactive intermediates. Furthermore, the comparable photosensitization properties of **MixL-AuNC** and the parent **DOP1-AuNC** were also confirmed using 1,3-diphenylisobenzofuran as a probe substrate for the generation of singlet oxygen (Figure S9).[6b,8] These results confirm that **MixL-AuNC** acts as a photosensitizer, generating singlet oxygen and catalytically active intermediates in the catalytic cycle.

DFT calculations

The intermediacy of the alkynyl-exchanged AuNCs was also confirmed through DFT calculations of the reaction pathway, using $[Au_{25}(SMe)_{17}(C{\equiv}CPh)]^-$ as the model system (Figure 4). As there are two ligand coordination sites on the staples, the apex and the core site,[19] two regioisomers of alkynyl-exchanged AuNCs were investigated. Isomer **A** bearing an alkynyl ligand at the apex site follows a thermodynamically favorable catalytic pathway that includes C–C bond formation, alkyne coordination, and subsequent deprotonation/alkynyl complexation steps. The highest activation barrier for C–C bond formation (**B**→**C**) of 12.0 kcal/mol is reasonable in the observed photocatalytic reaction at room temperature. After the C–C bond formation, the generated propargylamine acts as a bidentate ligand, stabilizing the surface Au atoms of the cluster **C** through coordination. After the coordination of the external alkyne, the bidentate nature of propargylamine enables the formation of an energetically favorable transition state $\mathbf{TS_{E\text{-}Pro}}$ for the subsequent deprotonation and alkynyl complexation step (**E**→**A** + product), with an activation barrier of 2.1 kcal/mol. In contrast to the apex site-exchanged isomer **A**, the core site-exchanged isomer **A**′ showed a slightly energetically unfavorable pathway. Although all core-site isomers have lower energies than the corresponding apex-site isomers, both alkyne coordination and deprotonation/alkynyl-complexation steps are thermodynamically unfavorable, with intermediate **D**′ being more stable than the alkyne-exchanged intermediate **E**′ and the final product, regenerated **A**′ and the ammonium salt of propargylamine. Recently, Teranishi et al. reported that the ligand-exchange

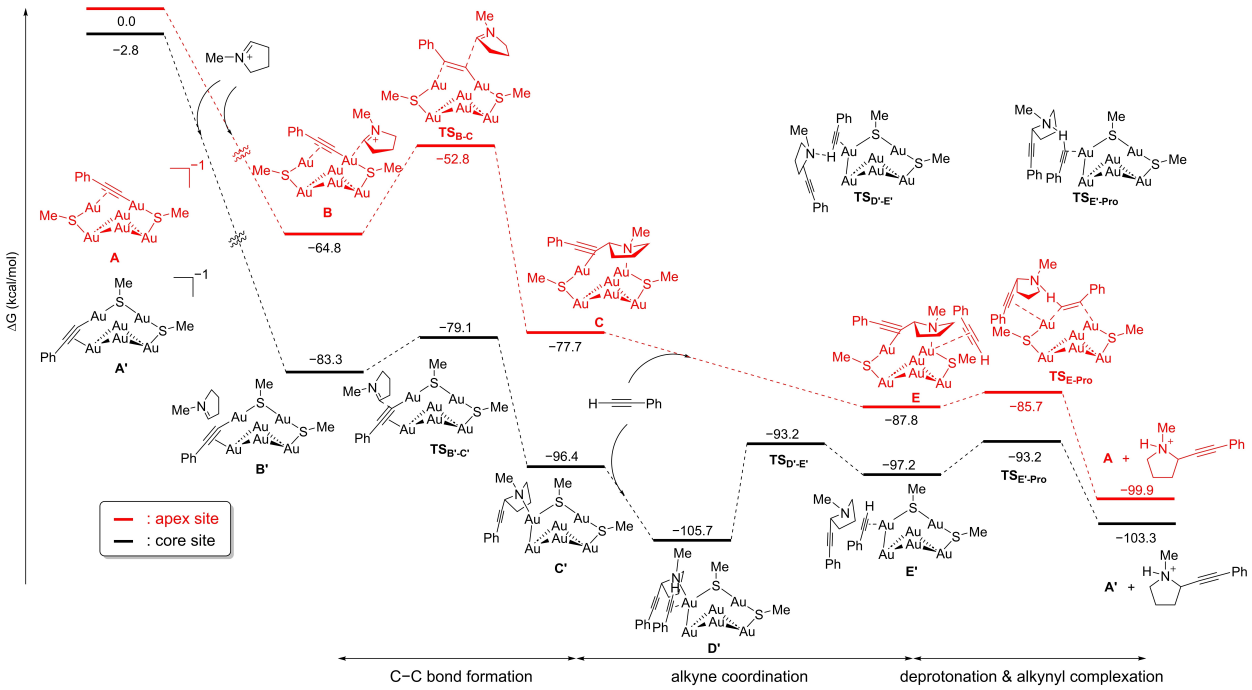

Figure 4. Density functional theory calculations depicting the reaction profiles of the $[Au_{25}(SMe)_{17}(C{\equiv}CPh)]^-$-mediated alkynylation via photocatalytically generated iminium intermediates. Partial molecular structures of AuNCs are shown for clarity.

reaction of $[Au_{25}(SR)_{18}]^-$ proceeds preferably at the apex site with sterically hindered thiols via kinetic control, despite the thermodynamic stability of the core site-exchanged regioisomers.[20] Similar to the reported results, the alkynyl exchange reaction in the current reaction predominantly occurs at the apex site through kinetic control, attributed to steric hindrance imposed by peptide dendron thiolates. Based on the thermodynamically favorable reaction pathway and kinetically favorable ligand-exchange reaction, it is highly likely that the apex site is primarily involved in the current reaction.

In addition, time-dependent density functional theory (TDDFT) calculations of both alkynyl-exchanged AuNCs **A** and **A′** suggest a negligible spectral change around 680 nm compared to the parent $[Au_{25}(SMe)_{18}]^-$ nanocluster (Figure S11), consistent with the observed absorption spectrum of the synthesized alkynyl-exhanged **MixL-AuNC** (Figure S8). During the catalytic cycle, the intermediates of the core-exchanged AuNCs showed slightly longer average Au_{core}-Au_{shell} and Au_{shell}-Au_{shell} distances than those of the apex-exchanged AuNCs because of the direct bonding of the reaction site to the Au_{13} superatomic core (Table S3). However, intermediates **A** and **A′** have almost the same average distance from Au_{core}-Au_{shell} and Au_{shell}-Au_{shell} to the parent $[Au_{25}(SMe)_{18}]^-$ nanocluster, resulting in a negligible change in the photophysical features of the Au_{13} superatomic core following ligand exchange. A negligible change was also observed in the frontier orbitals of both **A** and **A′**, with the HOMO and LUMO being triply degenerate superatomic 1P and doubly degenerate 1D orbitals, respectively, resembling those of the parent $[Au_{25}(SMe)_{18}]^-$ nanocluster (Figure S10). These results further support the intermediacy of alkynyl-exchanged AuNCs in the photosensitization cycle.

Based on our experimental and computational studies, we propose that the catalytic cycle is initiated by the formation of alkynyl-exchanged AuNCs (Figure 5). Similar to the original **DOP1-AuNC**, alkynyl-exchanged AuNC **A** is photoexcited by the 680 nm light, generating singlet oxygen. The photogenerated singlet oxygen reacts with the tertiary amine **1** via the SET/HAT pathway, leading to the formation of corresponding iminium cations and hydroperoxyl anions. AuNC **A** also reacts with the photogenerated iminium cation to form the propargylamine-coordinated AuNC intermediate **B** through C–C bond formation at the AuNC surface. The alkyne substrate then coordinates to AuNC **B**, facilitating the intramolecular deprotonation of the terminal alkyne with the neighboring propargylamine, ultimately generating the ammonium salt of propargylamine $[\mathbf{3}\text{-H}]^+$ and regenerating AuNC intermediate **A**, thereby completing the catalytic cycle. The ammonium salt $[\mathbf{3}\text{-H}]^+$ is neutralized by the hydroperoxyl anions, producing propargylamine **3** and hydrogen peroxide, which can be reduced by excess amine **1**, resulting in amine *N*-oxide and water.

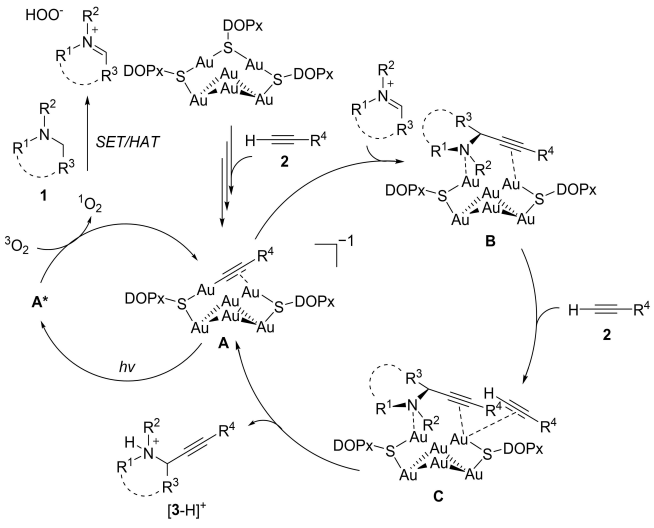

Figure 5. Proposed mechanism for photocatalytic cross-dehydrogenative coupling. Only the surface atoms of AuNCs are shown for clarity.

Conclusion

In conclusion, we have discovered the dual catalytic activity of $[Au_{25}(SR)_{18}]^-$ nanoclusters in the photocatalytic cross-dehydrogenative coupling between terminal alkynes and tertiary aliphatic amines. The reaction features the regioselective incorporation of diverse alkynyl substituents at the α-position of tertiary amines without requiring pre-functionalization, and it can be conducted under environmentally benign reaction conditions, utilizing visible light irradiation under an oxygen atmosphere. Two distinct structural components of $[Au_{25}(SR)_{18}]^-$ nanoclusters, namely the Au_{13} superatomic core and $Au_2(SR)_3$ staples, cooperatively participate in the coupling reaction as catalytic centers for photosensitized $^1O_2$ generation and C–C bond formation, respectively. Mechanistic investigations revealed that the in situ generated alkynyl-exchanged AuNCs act as catalytic intermediates, showing photosensitization activity similar to that of the original $[Au_{25}(SR)_{18}]^-$ nanocluster, indicating the retention of the Au_{13} superatomic core. The smooth catalytic turnover, coupled with a significantly reduced induction period, can be attributed to the structural modification of the staple moieties with an alkynyl ligand. This study underscores the potential of metallic nanoclusters as multifunctional catalysts by leveraging the cooperation of the superatomic core and surface-protecting organometallic moieties, thereby paving the way for the multistep synthesis of structurally complex functional molecules facilitated by a straightforward reaction setup.

Acknowledgements

This research received partial support from JSPS KAKENHI Grant Numbers JP23K17930, JP23KJ1383, The Kyoto University Foundation, Iketani Science and Technology Foundation, Proterial Materials Science Foundation, and Taiyo Nippon Sanso Corporation. K.I. is grateful for the support from Grant-in-Aid for JSPS Fellows. The iJURC at ICR, Kyoto University provided support for the FT-ICR-MS measurements. The computational resources necessary

for this study were provided by the SuperComputer System at ICR, Kyoto University.

Conflict of Interest

The authors declare no conflict of interest.

Data Availability Statement

The data that support the findings of this study are available in the supplementary material of this article.

Keywords: Cross-Dehydrogenative Coupling · Dual Catalysis · Gold Nanocluster · Intermolecular Interaction · Photocatalyst

[1] a) R. Jin, G. Li, S. Sharma, Y. Li, X. Du, *Chem. Rev.* **2021**, *121*, 567–648; b) Y. Du, H. Sheng, D. Astruc, M. Zhu, *Chem. Rev.* **2020**, *120*, 526–622; c) Q. Shi, Z. Qin, H. Xu, G. Li, *Nanomaterials* **2019**, *9*, 838; d) R. R. Nasaruddin, T. Chen, N. Yan, J. Xie, *Coord. Chem. Rev.* **2018**, *368*, 60–79; e) S. Yamazoe, K. Koyasu, T. Tsukuda, *Acc. Chem. Res.* **2014**, *47*, 816–824.

[2] a) T. Omoda, S. Takano, T. Tsukuda, *Small* **2021**, *17*, 2001439; b) T. Kawawaki, A. Ebina, Y. Hosokawa, S. Ozaki, D. Suzuki, S. Hossain, Y. Negishi, *Small* **2021**, *17*, 2005328; c) X. Ma, Y. Tang, G. Ma, L. Qin, Z. Tang, *Nanoscale* **2021**, *13*, 602–614; d) Z. Lei, X.-K. Wan, S.-F. Yuan, Z.-J. Guan, Q.-M. Wang, *Acc. Chem. Res.* **2018**, *51*, 2465–2474; e) R. Jin, C. Zeng, M. Zhou, Y. Chen, *Chem. Rev.* **2016**, *116*, 10346–10413.

[3] a) M. Zhu, C. M. Aikens, F. J. Hollander, G. C. Schatz, R. Jin, *J. Am. Chem. Soc.* **2008**, *130*, 5883–5885; b) M. W. Heaven, A. Dass, P. S. White, K. M. Holt, R. W. Murray, *J. Am. Chem. Soc.* **2008**, *130*, 3754–3755; c) Y. Negishi, Y. Takasugi, S. Sato, H. Yao, K. Kimura, T. Tsukuda, *J. Am. Chem. Soc.* **2004**, *126*, 6518–6519; d) T. G. Schaaff, G. Knight, M. N. Shafigullin, R. F. Borkman, R. L. Whetten, *J. Phys. Chem. B* **1998**, *102*, 10643–10646.

[4] a) T. D. Green, C. Yi, C. Zeng, R. Jin, S. McGill, K. L. Knappenberger Jr., *J. Phys. Chem. A* **2014**, *118*, 10611–10621; b) M. S. Devadas, J. Kim, E. Sinn, D. Lee, T. Goodson III, G. Ramakrishna, *J. Phys. Chem. C* **2010**, *114*, 22417–22423; c) S. A. Miller, J. M. Womick, J. F. Parker, R. W. Murray, A. M. Moran, *J. Phys. Chem. C* **2009**, *113*, 9440–9444.

[5] a) H. Hirai, S. Takano, T. Nakashima, T. Iwasa, T. Taketsugu, T. Tsukuda, *Angew. Chem. Int. Ed.* **2022**, *61*, e202207290; b) S. Takano, H. Hirai, T. Nakashima, T. Iwasa, T. Taketsugu, T. Tsukuda, *J. Am. Chem. Soc.* **2021**, *143*, 10560–10564; c) H. Shen, S. Xiang, Z. Xu, C. Liu, X. Li, C. Sun, S. Lin, B. K. Teo, N. Zheng, *Nano Res.* **2020**, *13*, 1908–1911; d) M. R. Narouz, S. Takano, P. A. Lummis, T. I. Levchenko, A. Nazemi, S. Kaappa, S. Malola, G. Yousefalizadeh, L. A. Calhoun, K. G. Stamplecoskie, H. Häkkinen, T. Tsukuda, C. M. Crudden, *J. Am. Chem. Soc.* **2019**, *141*, 14997–15002; e) Y. Shichibu, K. Konishi, *Small* **2010**, *6*, 1216–1220.

[6] a) S. Wang, L. Tang, B. Cai, Z. Yin, Y. Li, L. Xiong, X. Kang, J. Xuan, Y. Pei, M. Zhu, *J. Am. Chem. Soc.* **2022**, *144*, 3787–3792; b) H. Kawasaki, S. Kumar, G. Li, C. Zeng, D. R. Kauffman, J. Yoshimoto, Y. Iwasaki, R. Jin, *Chem. Mater.* **2014**, *26*, 2777–2788.

[7] M. Liu, L. Gao, L. Zhao, J. He, Q. Yuan, P. Zhang, Y. Zhao, X. Gao, *Sci. Rep.* **2017**, *7*, 131.

[8] K. Isozaki, R. Ueno, K. Ishibashi, G. Nakano, H. Yin, K. Iseri, M. Sakamoto, H. Takaya, T. Teranishi, M. Nakamura, *ACS Catal.* **2021**, *11*, 13180–13187.

[9] T. Nagata, Y. Adachi, Y. Obora, *Synlett* **2018**, *29*, 2655–2659.

[10] S. Li, H. Chen, X. Liu, H. Liu, J. Ma, Y. Zhu, *Chem. Sci.* **2020**, *11*, 8000–8004.

[11] a) Q. Li, A. Das, S. Wang, Y. Chen, R. Jin, *Chem. Commun.* **2016**, *52*, 14298–14301; b) Y. Adachi, H. Kawasaki, T. Nagata, Y. Obora, *Chem. Lett.* **2016**, *45*, 1457–1459.

[12] a) Y. Liu, X. Chai, X. Cai, M. Chen, R. Jin, W. Ding, Y. Zhu, *Angew. Chem. Int. Ed.* **2018**, *57*, 9775–9779; b) L. Sun, Y. Yun, H. Sheng, Y. Du, Y. Ding, P. Wu, P. Li, M. Zhu, *J. Mater. Chem. A* **2018**, *6*, 15371–15376.

[13] C. A. Hosier, I. D. Anderson, C. J. Ackerson, *Nanoscale* **2020**, *12*, 6239–6242.

[14] a) C. Grundke, R. C. Silva, W. R. Kitzmann, K. Heinze, K. T. de Oliveira, T. Opatz, *J. Org. Chem.* **2022**, *87*, 5630–5642; b) A. M. Nauth, E. Schechtel, R. Dören, W. Tremel, T. Opatz, *J. Am. Chem. Soc.* **2018**, *140*, 14169–14177.

[15] C. Ferroud, P. Rool, J. Santamaria, *Tetrahedron Lett.* **1998**, *39*, 9423–9426.

[16] Y. Shen, I. Funez-Ardoiz, F. Schoenebeck, T. Rovis, *J. Am. Chem. Soc.* **2021**, *143*, 18952–18959.

[17] E. L. Clennan, A. Pace, *Tetrahedron* **2005**, *61*, 6665–6691.

[18] P. Baillargeon, T. Lussier, Y. L. Dory, *J. Crystallogr.* **2014**, *2014*, 371629.

[19] Y. Niihori, Y. Kikuchi, A. Kato, M. Matsuzaki, Y. Negishi, *ACS Nano* **2015**, *9*, 9347–9356.

[20] W. Suzuki, R. Takahata, Y. Chiga, S. Kikkawa, S. Yamazoe, Y. Mizuhata, N. Tokitoh, T. Teranishi, *J. Am. Chem. Soc.* **2022**, *144*, 12310–12320.

Manuscript received: August 18, 2023
Accepted manuscript online: November 5, 2023
Version of record online: November 16, 2023